Biomedical Optics EXPRESS

Correlating light scattering with internal cellular structures

Oana C. Marina, Claire K. Sanders, and Judith R. Mourant*

MS M888, Bioscience Division, Los Alamos National Laboratory, Los Alamos, NM 87545, USA

*jmourant@lanl.gov

Abstract: The origins of side scattering from a fibroblast and cervical cell line were determined by comparing side-scatter images with images stained for lysosomes, nuclei, and mitochondria on a cell by cell basis. Lysosomes or nuclei are the most efficient type of scatterer depending on the cell type and incident light polarization. The relative scattering efficiencies of lysosomes and mitochondria were the same for both cell lines, while the scattering efficiencies of the nuclei differed. The percent of 90° scattering from the nucleus, mitochondria, and lysosomes as well as the group of other internal cellular objects was estimated. The nucleus was the largest contributor to side scatter in the cervical carcinoma cells. The contributions of lysosomes, mitochondria, the nucleus, and particles unstained by either Hoechst, LysoSensor or MitoTracker ranges from ∼20% to ∼30% in fibroblast cells. The contribution of lysosomes to side scatter was much stronger when the incident light was polarized perpendicular to the scattering plane than when the polarization of the side scatter laser was parallel to the scattering plane. This dependence on side scatter polarization indicates that lysosomes contain scattering structures that are much smaller than the wavelength of light used in the measurements (785 nm). In conclusion, mitochondria were not found to be either the most efficient scatterer or to have the largest contribution to scattering in either cell line, in contrast to previous reports. Rather lysosomes, nuclei and unknown particles all have significant contributions to 90° scattering and the contributions of some of these particles can be modulated by changing the polarization of the incident light.

OCIS codes: (170.0170) Medical optics and biotechnology; (290.0290) Scattering.

References and links

1. G. C. Salzman, J. M. Crowell, J. C. Martin, T. T.Trujillo, A.Romero, P. F. Mullaney, and P. M. LaBauve, "Cell classification by laser light scattering: identification and separation of unstained leukocytes," Acta Cytol. **19**, 374–377 (1975).
2. L. S. Cram and A. Brunsting, "Fluorescence and light-scattering measurements on hog cholera-infected PK-15 cells," Exp. Cell Res. **78**, 209–213 (1973).
3. J. Q. Brown, T. M. Bydlon, L. M. Richards, B. Yu, S. A. Kennedy, J. Geradts, L. G. Wilke, M. K. Junker, J. Gallagher, W. T. Barry, and N. Ramanujam, "Optical assessment of tumor resection margins in the breast," IEEE J. Sel. Top. Quantum Electron. **16**, 530–544 (2010).
4. S. C. Kanick, C. van der Leest, J. G. Aerts, H. C. Hoogsteden, S. Kascakova, H. J. Sterenborg, A. Amelink, "Integration of single-fiber reflectance spectroscopy into ultrasound-guided endoscopic lung cancer staging of mediastinal lymph nodes," J. Biomed. Opt. **15**, 017004 (2010).

#156183 - $15.00 USD Received 7 Oct 2011; revised 2 Dec 2011; accepted 30 Dec 2011; published 13 Jan 2012

5. J. R. Mourant, T. J. Bocklage, T. M. Powers, H. M. Greene, M. H. Dorin, A. G. Waxman, M. M. Zsemlye, and H. O. Smith, "Detection of cervical intraepithelial neoplasias and cancers in cervical tissue by in vivo light scattering," J. Low Genit. Tract. Dis.**13**, 216–223 (2009).
6. C. R. Weber, R. A. Schwarz, E. N. Atkinson, D. D. Cox, C. MacAulay, M. Follen, and R. Richards-Kortum, "Model-based analysis of reflectance and fluorescence spectra for in vivo detection of cervical dysplasia and cancer," J. Biomed. Opt. **13**, 064016 (2008).
7. R. A. Schwarz, W. Gao, D. Daye, M. D. Williams, R. Richards-Kortum, and A. M. Gillenwater, "Autofluorescence and diffuse reflectance spectroscopy of oral epithelial tissue using a depth-sensitive fiber-optic probe," Appl. Opt. **47**, 825–834 (2008).
8. Y. Zhu, T. Fearn, G. Mackenzie, B. Clark, J. M. Dunn, I. J. Bigio, S. G. Bown, and L. B. Lovat, "Elastic scattering spectroscopy for detection of cancer risk in Barrett's esophagus: experimental and clinical validation of error removal by orthogonal subtraction for increasing accuracy," J. Biomed. Opt.**14**, 044022 (2009).
9. B. Beauvoit, T. Kitai, and B. Chance, "Contribution of the mitochondrial compartment to the optical properties of the rat liver: a theoretical and practical approach," Biophys. J. **67**, 2501–2510 (1994).
10. A. Blouin, R. P. Bolender, and E. R. Weibel, "Distribution of organelles and membranes between hepatocytes and nonhepatocytes in the rat liver parenchyma. A stereological study," J. Cell Biol. **72**, 441–455 (1977).
11. A. M. James, Y.-H. Wei, C.-Y. Pang, and M. P. Murphy, "Altered mitochondrial function in fibroblasts containing Melas or Merrf mitochondrial DNA mutations," Biochem J. **318**, 401–407 (1996).
12. R. M. Pasternack, J.-Y. Zheng, and N. N. Boustany, "Optical scatter changes at the onset of apoptosis are spatially associated with mitochondria," J.Biomed.Opt. **15**, 040504 (2010).
13. J. D. Wilson, W. J. Cottrell, and T. H. Foster, "Index-of-refraction-dependent subcellular light scattering observed with organelle-specific dyes," J. Biomed. Opt. **12**, 014010 (2007).
14. I. Itzkan, L. Qui, H. Fang, M. M. Zaman, E. Vitkin, I. C. Ghiran, S. Salahuddin, M. Modell, C. Andersson, L. M. Kimerer, P. B. Cipolloni, K.-H. Lim, S. D. Freedman, I. Bigio, B. P. Sachs, E. B. Hanlon, and L. T. Perelman, "Confocal light absorption and scattering spectroscopic microscopy monitors organelles in live cells with no exogenous labels," Proc. Natl. Acad. Sci. U.S.A. **104**, 17255–17260 (2007).
15. J. R. Mourant, M. Canpolat, C. Brocker, O. Esponda-Ramos, T. M. Johnson, A. Matanock, K. Stetter, and J. P. Freyer, "Light scattering from cells: the contribution of the nucleus and the effects of proliferative status," J. Biomed. Opt. **5**, 131–137 (2000).
16. W. E. Ortyn, B. E. Hall, T. C. George, K. Frost, D. A. Basiji, D. J. Perry, C. A. Zimmerman, D. Coder, and P. J. Morrissey, "Sensitivity measurement and compensation in spectral imaging," Cytometry A **69**, 852–862 (2006).
17. J. R. Mourant, T. M. Johnson, S. Carpenter, A. Guerra, T. Aida, and J. P. Freyer "Polarized angular dependent spectroscopy of epithelial cells and epithelial cell nuclei to determine the size scale of scattering structures," J. Biomed. Opt. **7**, 378–387 (2002). .
18. A. E. Frazier, C. Kiu, D. Stojanovski, N. J. Hoogenraad, and M. T. Ryan, "Mitochondrial morphology and distribution in mammalian cells," Biol. Chem. **387**, 1551–1558 (2006).
19. J. Heuser, "Changes in lysosome shape and distribution correlated with changes in cytoplasmic pH," J. Cell. Biol. **108**, 855–864 (1989).
20. V. I. Korolchuk , S. Saiki, M. Lichtenberg, F. H. Siddiqi, E. A. Roberts, S. Imarisio, L. Jahreiss, S. Sarkar, M. Futter, F. M. Menzies, C. J. O'Kane, V. Deretic, and D. C. Rubinsztein, "Lysosomal positioning coordinates cellular nutrient responses," Nature Cell Biol. **13**, 453–460 (2011).
21. T. M. Johnson and J. R. Mourant, "Polarized wavelength-dependent measurements of turbid media," Opt. Express **4**, 200–216 (1999).
22. G. C. Salzman, "Light scatter: detection and usage," Curr. Protoc. Cytom.**9**, 1.13.1 (1999).
23. N. Demaurex, "pH homeostasis of cellular organelle," News Physiol. Sci. **17**, 1–5 (2002).
24. D. Watson, N. Hagen, J. Diver, P. Marchand, and M. Chachisvilis, "Elastic light scattering from single cells: orientational dynamics in optical trap," Biophys. J. **87**, 1298–1306 (2004).
25. D. Arifler, M. G. A. Carraro, A. Malpica, M. Follen, and R. Richards-Kortum, "Light scattering from normal and dysplastic cervical cells at different epithelial depths: finite-difference time-domain modeling with a perfectly matched layer boundary condition," J. Biomed. Opt. **8**, 484–494 (2003).
26. J.D. Wilson and T.H. Foster, "Characterization of lysosomal contribution to whole-cell light scattering by organelle ablation," J. Biomed. Opt. **12**, 030503 (2007).
27. P. K. Kennady, M. G. Ormerod, S. Singh, and G. Pande, "Variation of mitochondrial size during the cell cycle: a multiparameter flow cytometric and microscopic study," Cytometry Part A **62A**, 97–108 (2004).
28. P. Saftig, *Lysosomes* (Springer-Verlag, 2005).
29. J. M. Schmitt and G. Kumar, "Optical scattering properties of soft tissue: a discrete model," Appl. Opt. **37**, 2788–2797 (1998).
30. J. D. Wilson and T. M. Foster, "Mie theory interpretations of light scattering from intact cells," Opt. Lett. **30**, 2442–2444 (2005).

#156183 - $15.00 USD Received 7 Oct 2011; revised 2 Dec 2011; accepted 30 Dec 2011; published 13 Jan 2012

1. Introduction

Light scattering measurements provide information about cells without the need for stains or other perturbation that might affect the cell or hinder subsequent measurements. Work in the 1970's demonstrated that light scattering properties are related to cell morphology [1, 2]. Recently, this fact has motivated the development of *in vivo* light scatter techniques for non-intrusive diagnosis of precancerous conditions. Clinical trials on several different tissue or organ sites have been reported: breast, lymph nodes, cervical tissue, oral tissue, and esophageal tissue [3–8]. In developing light scattering techniques, it is helpful to understand the origin of light scattering. A fundamental question is: What physical features of the cell are scattering light? Many indirect and a few direct measurements have been performed. Early work by Beauvoit *et al.* demonstrated that mitochondria are a major contributor to light scattering from liver cells [9]. However, these results can not be extrapolated to other cell types. Hepatocytes are unusual in that mitochondria make up 28% of the cell volume [10]. In other cell types, mitochondria are much less of the cell volume. For example, in human skin fibroblasts, mitochondria are 2.4% and lysosomes are more than 2.7% of the cell volume [11].

To investigate what structures scatter light, some investigators have taken the approach of modifying one type of organelle and then measuring whether the light scattering properties changed. Changes in light scattering have been correlated with both alterations in lysosomes and mitochondria. The locations of light scatter changes in bovine aortic endothelial cells treated with staurosporine (an inducer of apoptosis) have been demonstrated to be correlated with the location of MitoTracker Green fluorescence from mitochondria [12]. Light scatter from lysosomes has been modulated in EMT6 cells. The addition of a strong absorber that localizes in lysosomes was shown to reduce angular light scattering between the angles of 15° - 60° [13]. This information is used in fitting the angular dependent light scattering of a cell to a trimodal distribution in which three distributions are identified, one with a mean of 0.6 μm being the lysosomes, a second distribution with a mean of 0.2 μm that is assigned to secretory granules and a third distribution with a mean of 1.3 μm that is assigned to mitochondria. This third distribution was reported to be responsible for 80% of the scattering. Another method of measuring scattering from subcellular particles is CLASS (confocal light absorption and scattering spectroscopic) microscopy [14]. In CLASS microscopy the organelle properties of a small volume are extracted from the measured spectrum of that confocal volume by data fitting. In a test of CLASS microscopy, an image of lysosomal fluorescence in a single cell was compared to the CLASS microscopy reconstruction of the location of lysosomes within the cell [14]. There is a correlation between the two techniques, but the CLASS microscopy shows lysosomes in some locations where they are not seen in the fluorescent image.

The approach taken here is to image side scatter and organelle specific fluorescence simultaneously for thousands of cells. The images can then be examined to determine if scattering is correlated with any particular organelle. 90° fluorescence from mitochondria, lysosomes, and nuclei was simultaneously acquired with side scatter images.

2. Methods

2.1. Cell culture

MR1 rat fibroblast cells and SiHa human epithelial cells were each maintained in monolayer culture using standard mammalian cell culture at 37°C. MR1 cells were grown in Dulbecco's Modified Eagles Medium (DMEM) supplemented with 5% (v/v) of fetal calf serum (HyClone Thermo Fisher Scientific, Waltham, MA) and SiHa cells were grown in αMEM supplemented with 10% (v/v) of fetal calf serum (HyClone Thermo Fisher Scientific, Waltham, MA). Both media were further supplemented with 100 units/ml of Penicillin, and 100 μg/mL of Strepto-

#156183 - $15.00 USD Received 7 Oct 2011; revised 2 Dec 2011; accepted 30 Dec 2011; published 13 Jan 2012

mycin. To obtain cell suspensions for staining and subsequent flow cytometric analysis, cells were harvested from monolayer cultures by treatment with 0.25% trypsin in a phosphate-buffer (pH 7.4) containing 1 mM EDTA and 25mM HEPES. Immediately after harvesting complete medium was added to the cells. The cells were counted using a hemocytometer.

We have previously shown that light scattering depends on the proliferation status of the cells with light scatter above $\sim 50^{\circ}$ increasing with greater DNA content [15]. The proliferative status of the cells was determined by fixing 10^6 cells in 70% ethanol and 30% PBS and stored at -20° C at least over night. The fixed cells samples were centrifuged at $140\times$g for 5 minutes and the ethanol was removed by aspiration. The pelleted cells were then resuspended in a 1 mL solution of PBS (HyClone Thermo Fisher Scientific, Waltham, MA) containing 5 μg/mL propidium iodide and 50 μg/mL of RNase A (both from Sigma Aldrich, St. Louis, MO). The cells were then incubated at 37°C for 30 min. and analyzed with a FACSCalibur flow cytometer (Becton-Dickinson, Franklin Lakes, NJ), using 15 mW 488 nm excitation, with fluorescence emission collected through a 650 nm longpass filter. Data were analyzed with ModFit LT (Verity Software House, Topsham, ME) to determine cell cycle distributions after debris and aggregates were gated out. The SiHa cells were in the late exponential stage of growth with $\sim$70% of the cells in G1, $\sim$20% of the cells in S-phase and $\sim$10% of the cells in G2. The proliferative status of the MR1 cells was variable ranging from exponential to plateau.

2.2. Cell staining

Hoechst 33342 (H1399) was used to stain the nuclei. It is a live cell stain which binds double stranded DNA. MitoTracker Orange CMTMRos (M7510) was used to stain mitochondria. This dye concentrates in the mitochondria of live cells. LysoSensor Green DND-189 (L-7535) was used for staining lysosomes. This dye has a pKa of $\sim$ 5.2 and accumulates in acidic organelles as the result of protonation. This protonation also results in an increase in fluorescence intensity. All dyes were purchased from Invitrogen (Eugene, OR).

MR1 and SiHa cells were suspended in DMEM and αMEM complete media, respectively, at a concentration of 10^6 cells/mL. All cell staining was performed at room temperature with the room lights off. The cells were first incubated in 32 μM Hoechst 33342 for 15 minutes. Subsequently, the cells were incubated in 80 nM LysoSensor dye for 5 minutes. Next, the cell suspension was incubated with 584 nM MitoTracker Orange CMTMRos for 5 minutes. To remove any unbound dyes, 10 mL PBS was added to the cell suspension, the cells were centrifuged for 5 minutes at $320\times$g and the supernatant was removed. The cell pellet was gently resuspended in 200 μL DMEM or αMEM complete media and treated again with Hoechst 33342 dye (6.4μM). Roughly 10 minutes after the staining was complete, the cells were analyzed by flow cytometry.

2.3. Flow cytometric imaging

Flow cytometry imaging was performed using an ImageStream^X flow cytometer (Amnis Corporation, Seattle, WA). A schematic of the instrument is shown in Fig. 1. As a cell passes through the laser beam, a plane of the cell is imaged using a time-delay integration CCD. Each pixel in the raw data images is 0.5x0.5μm. A 0.75 NA, 40x collection objective with a 4 μm depth of field was used and data were collected using INSPIRE 4.0 Software. All images were obtained at 90° from the incident excitation except the brightfield image which was obtained in the standard straight through geometry. Hoechst 33342 was excited with the 405 nm laser and its emission was detected through a 430-505 nm filter, MitoTracker Orange was excited with the 488 nm laser and its emission was collected from 595-660 nm. LysoSensor Green was also excited with the 488 laser with 480-560 nm emission. (The Amnis flow cytometer has a 488 nm notch filter over all detection channels [16].) A linearly polarized 785nm laser was used to mea-

#156183 - $15.00 USD Received 7 Oct 2011; revised 2 Dec 2011; accepted 30 Dec 2011; published 13 Jan 2012

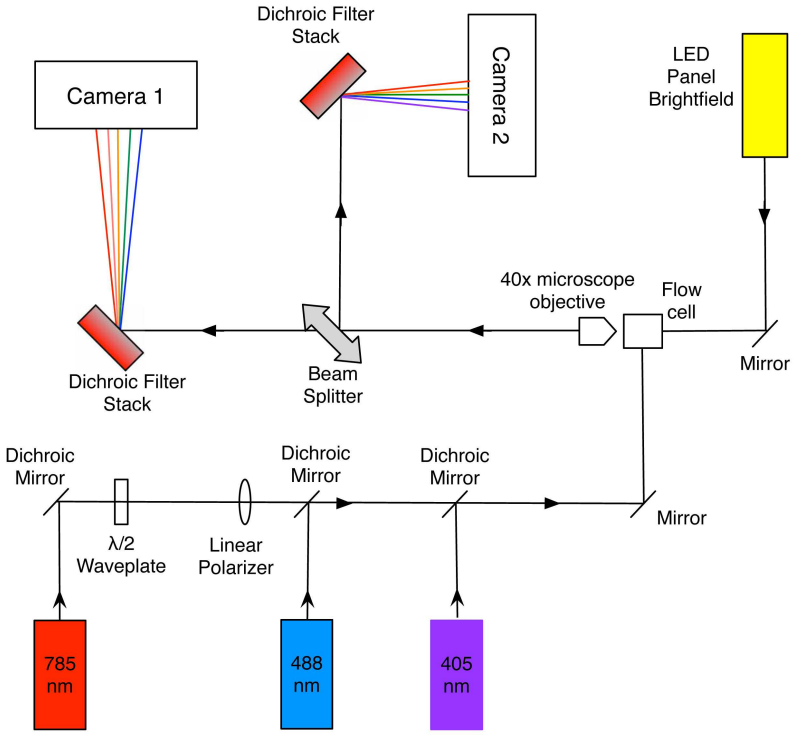

Fig. 1. Schematic of the parts of the optical train in the Amnis flow cytometer that we used. The $\lambda/2$ waveplate and the linear polarizer were only inserted into the instrument when measurements were made with the polarization of the 785 nm light scattering laser perpendicular to the scattering plane. Camera 1 was used for the brightfield, lysosomal and mitochondrial images while camera 2 collected the nuclear images.

sure side scatter. The polarization of the 785 nm laser beam is normally in the plane containing the excitation and light collection pathways. Previous work [17] has shown that side scatter depends strongly on the polarization of the laser beam. Consequently data were also taken with the polarization rotated 90°. This was achieved by inserting a $\lambda/2$ waveplate followed by a linear polarizer into the beam path of the 785 nm laser. The 785 nm laser was set to 5 mW for parallel polarization and 8 mW for perpendicular, this allowed for similar illumination intensities at the flow cell. Compensation (e.g., correcting for the fluorescence of LysoSensor in the Hoechst channel) was performed using the semi-automated procedure provided in the IDEAS Software that requires data from individually stained samples [16].

2.4. Image and data analysis

A combination of the IDEAS software provided by Amnis Corporation and Igor Pro (Wavemetrics, Portland, OR) and was used for data and image analysis. Images of single, in focus cells were selected for analysis. For each flow cytometry sample more than 1500 cells were used in the analysis.

Regions of a cell with a specific fluorescence are defined by masks in the IDEAS software. Fig. 2 shows example images and masks for one cell. The yellow lines are the outline of the mask used for the cell. Outlines of masks specifying regions of intense fluorescence are shown in green, orange, and purple on the LysoSensor, MitoTracker, and Hoechst images. The black

#156183 - $15.00 USD Received 7 Oct 2011; revised 2 Dec 2011; accepted 30 Dec 2011; published 13 Jan 2012

lines outline masks for regions in which the fluorescence of that image did not overlap with the fluorescence of other dyes. The outline of a region without any strong fluorescence is shown in red on the side scatter image. These masks were used in the quantification of the image data.

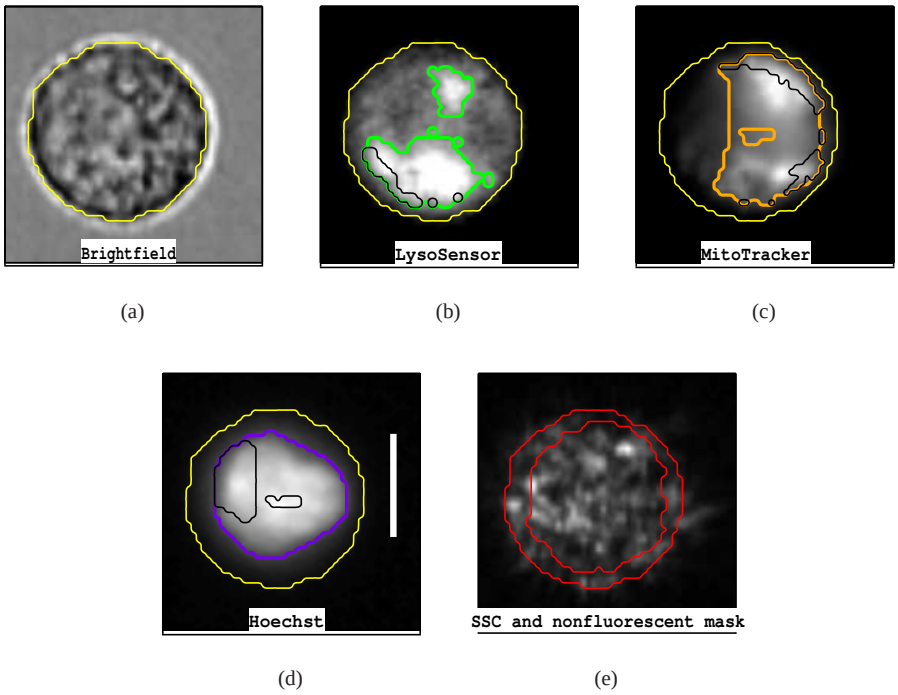

Fig. 2. Example raw images: a) Brightfield b) Lysosomes c) Mitochondria d) Nuclei e) Side scatter (SSC). The yellow lines are the outline of the mask used for the cell. Other colored lines are the outlines of masks covering areas where the dye fluorescence is considered significant. Black lines are the outlines of regions where only the dye in that image fluoresces. The mask for the non-fluorescent regions is shown on the SSC image. The thick white line on the Hoechst image has a length of 10μm.

Organelle scattering efficiency defined as the intensity of scattering per image area is calculated because it does not depend on organelle concentration and consequently may be applicable to a wide variety of cells. The calculation of scattering efficiency for the nucleus is given by Eq. 1. Only Hoechst fluorescing regions without overlap from regions under the LysoSenser or MitoTracker masks were used in the calculation, e.g. the regions outlined in black in Fig. 2. Analogous calculations were done for lysosomes, mitochondria, non-fluorescent regions, and regions where both lysosomes and mitochondria fluoresced. The analogous calculation for the whole cell is shown in Eq. 2. The data were corrected for the fact that Hoechst staining increased cell scattering as described in Section 3.2. Although scattering efficiency is calculated as intensity/area, the units are really intensity/volume because the fluorescence is measured with a depth of field of 4 μm.

$$nuclear\ scattering\ efficiency = \frac{I_{scat}(nuclear\ region)}{Area(nuclear\ region)} \tag{1}$$

#156183 - $15.00 USD Received 7 Oct 2011; revised 2 Dec 2011; accepted 30 Dec 2011; published 13 Jan 2012

$$cell\ scattering\ efficiency = \frac{I_{scat}(Cell)}{Area(Cell)} \tag{2}$$

Estimates of the percent of side scatter for each of the measured cell constituents, lysosomes, mitochondria, nuclei, and unstained components were made for the case of a non-imaging measurement where scattering is collected from the entire cell. To estimate the percent of scattering from the nucleus, the area of the image that is the nucleus, as defined by the nuclear mask, was determined and an effective nuclear radius was calculated by assuming the nucleus was spherical. Similarly, an effective radius for the cell was estimated by assuming the cell was spherical and using the area of the mask for the brightfield image. The percent of scattering from the nucleus was then calculated by expression 3.

$$\frac{nuclear\ scattering\ efficiency}{cell\ scattering\ efficiency} \times \frac{nuclear\ volume}{cell\ volume} \times 100 \tag{3}$$

The area of images from which lysosomes are the major source of scattering were estimated by taking the area of only lysosomal fluorescence and adding 1/2 of the area that had both lysosomal and mitochondrial fluorescence but no nuclear fluorescence. The corresponding volume was calculated by constructing an annulus halfway between the nucleus and cell boundaries that had the same area and then calculating the volume of between two spheres with the diameters of the inner and outer diameters of the annulus. The analogous calculation was performed for mitochondria. To estimate the contribution to scattering of nonfluorescent objects, the area of the image for which there was no fluorescence was determined and then that area was converted into a volume in the same manner as was used for mitochondria and lysosomes.

3. Results

3.1. Raw images

Images from one cell are shown in Fig. 2. The brightfield image, (a), is used to define the outline of the cell for data analysis. The LysoSensor image (b) has a diffuse background which was present in many but not all cells. The LysoSensor mask is outlined in green and represents the area of intense LysoSensor fluorescence. The MitoTracker image (c) has less background and shows more structure within the area defined by the MitoTracker mask. Higher resolution images of mitochondria in fibroblast cells show a thread-like pattern with some dense areas within the cytoplasm [18] and our results are consistent with this result. The nuclear image for this particular cell is more diffuse than the majority of Hoechst images we obtained, but still shows a well-defined nucleus. Finally, the SSC images show significant structure which will be discussed later. Superimposed on the SSC image is the outline of a mask of a region that is not covered by any of the masks for LysoSensor, Hoechst or MitoTracker. We commonly, found that there was a nonfluorescent region near the edge of the cell. Lysosomes normally cluster around the cell center but move to the cell edge if the pH is decreased [19, 20]. Therefore, the edge of the cell is expected to be free of both Hoechst and LysoSensor fluorescence.

3.2. Side effects of staining

Data from singly stained and unstained samples were used to determine if the stains were affecting any properties of the cells that were to be measured for the triply stained samples. Based on literature searches and information about the dyes, no effects were expected. However, there were some surprises.

Average side scatter light intensity for unstained, singly, and triply stained cells for each experiment are shown in Figure 3. Cells were harvested for MR1 experiments on 7 different

#156183 - $15.00 USD Received 7 Oct 2011; revised 2 Dec 2011; accepted 30 Dec 2011; published 13 Jan 2012

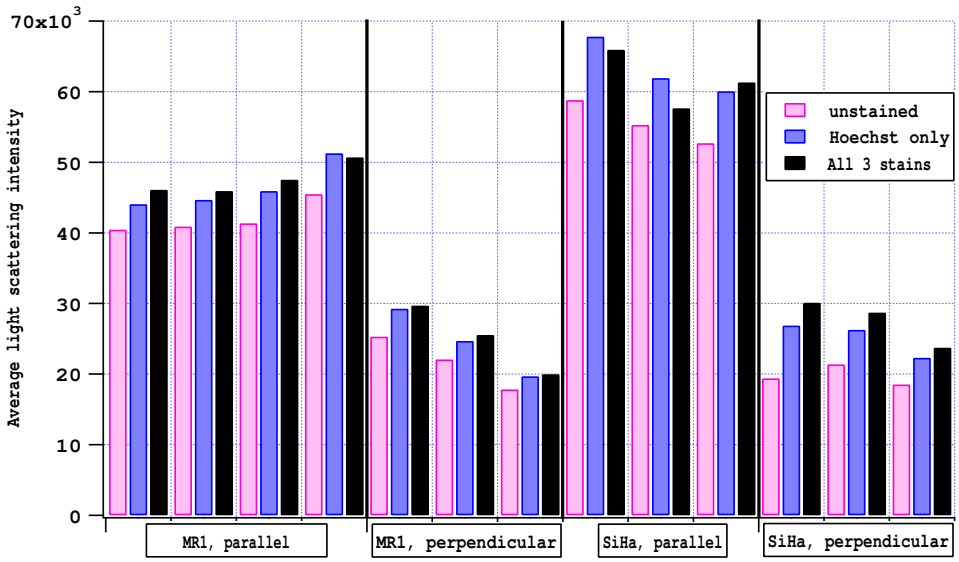

Fig. 3. Effects of cell staining on light scattering for 4 types of experiments.

days. On four of those days light scattering was measured with polarization of the incident light parallel to the scattering plane and three days the light scattering was performed with the polarization perpendicular to the scattering plane. Similarly SiHa cells were harvested on 6 different days and half the experiments used parallel polarization while the other half used incident light polarized perpendicular to the scattering plane. The graph shows strong evidence for increased scattering for Hoechst and triply stained cells as compared to unstained cells. We performed paired t-tests on the average results to determine if the increases in scattering were significant. At the 95% significance level, all changes between unstained and Hoechst stained cells were significant, but not all changes between unstained and triply stained cells were signficant. Table 1 shows the average change in scattering for each experiment type. The change in scattering upon Hoechst staining was verified using a standard flow cytometer - FACSCalibur flow cytometer (Becton-Dickinson, Franklin Lakes, NJ). The mean side scatter for MR1 cells stained with Hoechst increased by 9% same as for the Amnis imaging flow cytometer.

Comparisons of unstained cells to cells stained with only LysoSensor Green or MitoTracker Orange showed no significant changes at the 95% level, except for SiHa cells interrogated with parallel polarization in which the stained cells had decreased scattering (data not shown). This change was quite small, 4.5 ± 0.6 %. Consequently, the data analysis does not compensate for any effect of LysoSensor Green or MitoTracker Orange on light scattering.

Our data analysis accounts for the changes in scattering due to Hoechst staining. The total intensity of scatter from cells calculated from stained images, I_{scat}(cells), is multiplied by the fraction, f, given in Table 1. The change in scattering is assumed to be only due to scattering from the nucleus. Scattering from nuclear regions is calculated as in expression 4, where all scattering intensities are obtained from stained images. $I_{scat}(Cell)$ is the side scattering intensity from the whole cell defined by masks such as those in Fig. 2a. $I_{scat}(nucleus)$ is the intensity of side scattering from the Hoechst stained region define by masks such as the one outlined in purple in Fig 2d. $I_{scat}(cytoplasm)$ is $I_{scat}(Cell)$ minus $I_{scat}(nucleus)$. $I_{scat}(nuclear\ region)$ is the

#156183 - $15.00 USD Received 7 Oct 2011; revised 2 Dec 2011; accepted 30 Dec 2011; published 13 Jan 2012

side scatter intensity from the region of the cell for which only Hoechst fluoresces - an example mask is outlined in black in Fig. 2d. The fraction, f, multiplying $I_{scat}(cells)$ is the inverse of the factor by which nuclear scattering changes upon staining.

$$I_{scat}(nuclear\ region)\frac{(fI_{scat}(Cell)-I_{scat}(Cytoplasm))}{I_{scat}(nucleus)} \tag{4}$$

Table 1. Scattering of unstained samples relative to Hoechst stained samples

Experiment type	Fraction, f, of scattering of Hoechst stained samples exhibited by unstained samples
MR1 parallel polarization	0.915
MR1 perpendicular polarization	0.889
SiHa parallel polarization	0.874
SiHa perpendicular polarization	0.789

Cell size, as determined from the brightfield images, and nuclear size, as determined from the Hoechst stained area, were also compared for different staining conditions. The stains had no effect on either cell or nuclear size for the MR1 cells. Hoechst alone had no effect on size of the SiHa cells, but staining with all three stains did decrease the size of the cells (p = 0.0059) by $\sim$7% as compared to unstained cells. There was also a significant (p = 0.0028), but very small decrease (2%) in the size of the nuclei of SiHa cells stained with all three dyes as compared to Hoechst only stained cells.

3.3. Spatial overlap of fluorescence

Some overlap of the fluorescence of the mitochondrial, lysosomal and nuclear stains is expected in a nonconfocal image. To quantify the fluorescence overlap in each of the more than1500 cells, we used the similarity function provided in the IDEAS software. Similarity is defined by Eq. 5, where r is Pearson's correlation coefficient of the corresponding pixel intensities from two organelle specific fluorescence images of a single cell. When two parameters correlate, similarity is positive. When two parameters are anticorrelated, the similarity is negative.

$$similarity = ln(\frac{1+r}{1-r}) \tag{5}$$

The similarity of Hoechst and LysoSensor fluorescence in a region of the cell image where one or both of them fluoresce was calculated for each cell. Analogous calculations were done for the Hoechst and MitoTracker fluorescence as well as for LysoSensor and MitoTracker. Examples from an experiment with MR1 cells are shown in Fig. 4. For the vast majority of cells the fluorescence of MitoTracker and Hoechst anticorrelate. Also, for most cells, the fluorescence of LysoSensor and Hoechst is anticorrelated. The fluorescence of MitoTracker and LysoSensor frequently correlate due to the low resolution of the images. These results are representative of all of the experiments performed. Means and standard deviations of the similarities for the 3-4 experiments of each type are shown in Fig. 5. The consistency of results indicates that the staining did not vary due to cell type or during the course of the experiments.

3.4. Organelle scattering efficiency

Organelle scattering efficiency versus cell scattering efficiency is shown for one experiment using SiHa cells with the 785 nm scattering laser polarized parallel to the scattering plane

#156183 - $15.00 USD Received 7 Oct 2011; revised 2 Dec 2011; accepted 30 Dec 2011; published 13 Jan 2012

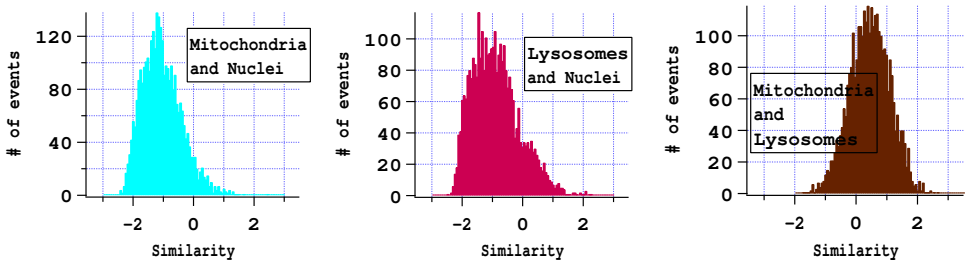

Fig. 4. Correlation of fluorescence intensities in the images from one experiment with MR1 cells. a) The similarity of mitochondrial and nuclear fluorescence demonstrates that mitochondrial fluorescence is weak where nuclear fluorescence is strong and vice versa. b) Similarity of lysosomal and nuclear fluorescence demonstrates that for most cells lysosomal fluorescence is weak where nuclear fluorescence is strong and vice versa. c) The similarity of mitochondrial and lysosomal fluorescence shows that for many cells the location of mitochondrial and lysosomal fluorescence overlaps significantly.

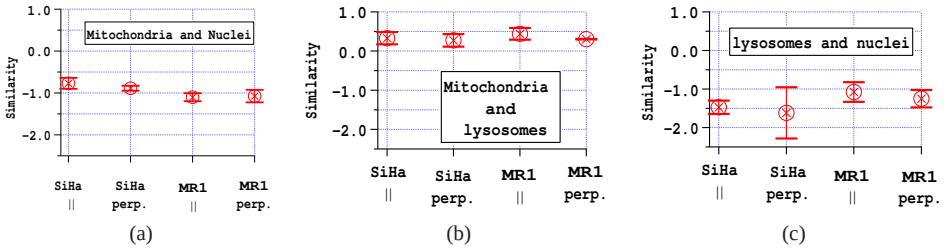

Fig. 5. Mean and standard deviation of the average similarity between the fluorescence of two dyes. a) Similarity of Hoechst and MitoTracker Orange fluorescence. b) Similarity of LysoSensor Green and MitoTracker Orange fluorescence. c) Similarity of Hoechst and MitoTracker Orange fluorescence. Results are for 3 each of the SiHa experiments and for 3 experiments with MR1 cells using parallel polarization and 4 experiments with perpendicular polarization.

in Fig 6. These results show that for this particular experiment, scattering from cell regions showing only LysoSensor fluorescence (green) scattered with roughly the same efficiency as the cell on average. Scattering from regions with only MitoTracker fluorescence (orange) scattered less efficiently and non-fluorescent regions (black) were on average the least efficient. Regions emitting only Hoechst fluorescence (purple) scattered with slightly higher efficiency than the cell on average. Finally, a cell region was defined which include areas where only LysoSensor fluoresced and areas where only MitoTracker fluoresced as well as areas where LysoSensor and MitoTracker fluorescence overlapped. Scattering from these MitoTracker and LysoSensor emitting regions (brown) appears to be slightly less efficient than those with only LysoSensor fluorescence.

Measurements of absolute scattering efficiencies or scattering cross sections are quite difficult and were not possible with the instrumentation used. Therefore, our scattering must be plotted either with arbitrary units or relative to something. Fig. 7 shows scattering efficiencies plotted relative to the scattering efficiency of the entire cell. The ratios of scattering efficiencies

#156183 - $15.00 USD Received 7 Oct 2011; revised 2 Dec 2011; accepted 30 Dec 2011; published 13 Jan 2012

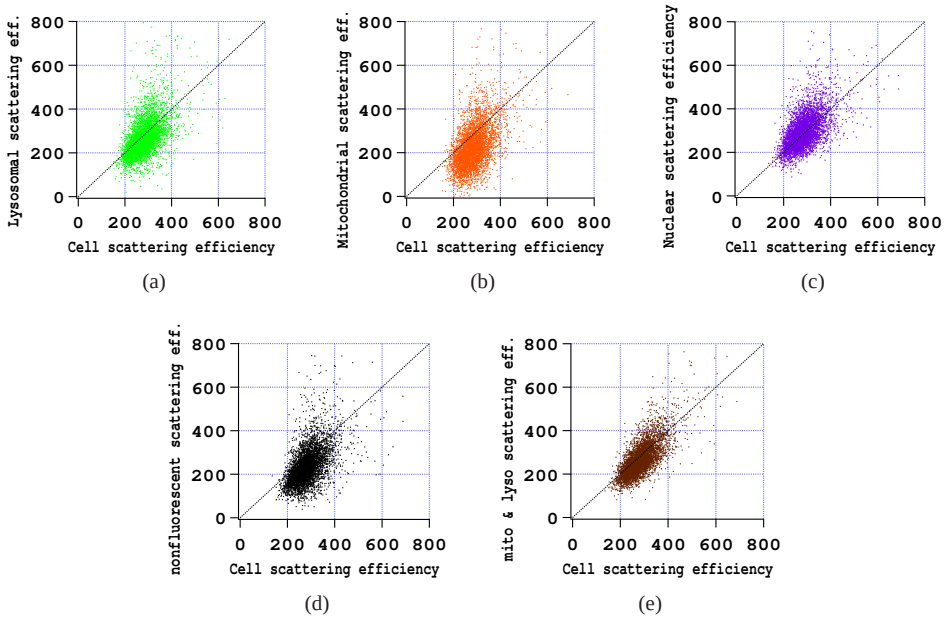

Fig. 6. Scattering efficiencies of cell regions stained only with specific dyes or in one case (d) with no fluorescence compared to the total cell scattering efficiency on a cell by cell basis. Results are for SiHa cells with the 785 nm light scattering laser polarized parallel to the scattering plane. a) LysoSensor. b) MitoTracker. c) Hoechst. d) Nonfluorescent. e) MitoTracker, LysoSensor or both.

(region/cell) were calculated on a cell by cell basis. Histograms demonstrated that the distributions of relative efficiencies were not symmetric and had a tail that resulted in the mean being consistently higher than the median. The distribution of values was likely due to both instrumental and biological effects and is discussed in more detail in the discussion section. To assure that the tail of the distribution was not confounding our results, both the mean and the median of the distributions of scattering efficiency ratios were computed. Only the median is shown in Fig. 7. These results clearly show that mitochondria are not the most efficient scatterer when the incident light polarization is perpendicular to the scattering plane.

To facilitate comparison of data obtained for different cell types and with different scattering polarizations, the data in Fig. 7 and similar data were divided by the average results for mitochondrial scattering efficiency. Fig. 8 shows the mean and median of the distribution of scattering efficiencies of various regions of the cell relative to the mean (or median) scattering efficiency of mitochondria. The top two figures, Figs. 8a and b are results obtained with the 785 nm laser polarized parallel to the scattering plane, and the two bottom figures, Figs. 8c and d are results obtained with the 785 nm laser polarized perpendicular to the scattering plane. The right figures are averages of the medians calculated for each experiment while the left figures are averages of the means calculated for each experiment. The open symbols shown for the nuclei indicate the error associated with correcting the scattering efficiency of the nucleus due to Hoechst staining discussed in Section 3.2.

A striking result of Figs. 8a and b is the weak scattering from the nucleus of the MR1 cells. Clearly, the nucleus of MR1 cells does not scatter light at 90° as efficiently as the cytoplasm. A second result of Figs. 8a and b is that the relative scattering efficiency of lysosomes, mitochon-

#156183 - $15.00 USD Received 7 Oct 2011; revised 2 Dec 2011; accepted 30 Dec 2011; published 13 Jan 2012

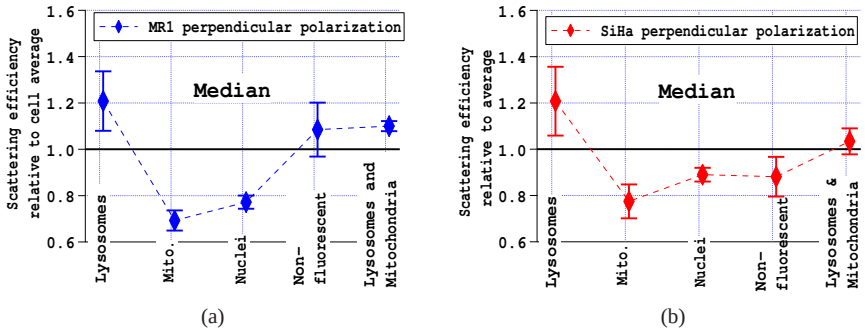

(a) (b)

Fig. 7. Medians of distributions of scattering efficiencies divided on a cell by cell bases by the scattering efficiency of the cell. The data points and error bars are the averages and standard deviations of the medians from three separate experiments each with more than 1500 cells.

dria, and non-fluorescent regions is the same for MR1 and SiHa cells. It is only the scattering efficiency of the nucleus that differs between the two cell lines.

From light scattering theory, it is known that scattering of light with the polarization perpendicular to the scattering plane will be at least as intense or more intense than scattering with the polarization parallel to the scattering plane. For a distribution of large particles ($\gtrsim 1\mu$m), scattering will be independent of polarization [21]. For small particles, scattering is greater when the polarization is perpendicular to the scattering plane (see for example [22]). Figs. 8c and d demonstrate that the scattering efficiency of lysosomes increases more than that of mitochondria. It appears that the non-fluorescent particles in SiHa cells differ from those in MR1 cells, because the scattering increases more when the polarization is changed for MR1 cells, than for SiHa cells. The changes in scattering efficiency with incident light polarization provide information on the morphology of the scattering structures. Compared to the scattering efficiency of mitochondria, the scattering efficiencies of all objects measured increases when the polarization is changed from parallel to perpendicular. (Note the change in scale between Figs. 8c and d and Figs. 8a and b.) Therefore, the scattering structures in mitochondria are on average larger than for the other organelles/objects. The increase in scattering efficiency is greatest for lysosomes demonstrating that lysosomes contain a large number of highly scattering small ($\lesssim$100 nm) particles.

We hypothesize that the relative scattering efficiency of lysosomes and mitochondria does not vary between cells types, but that the scattering of the nuclei or of other unstained structures may. This hypothesis can be checked by taking the ratio of lysosomal and mitochondrial scattering efficiencies and seeing if they are the same for MR1 and SiHa cells. In Fig. 8b and d population ratios were calculated. In Fig. 9 the ratio of scattering efficiencies was calculated on a cell-by-cell bases and then the ratios were averaged for each experiment. If there was no cell to cell variability, the results would be the same for both calculations. Figs. 8 and 9 demonstrate that there are some minor differences in results depending on whether population ratios or cell-by cell ratios are calculated, but the conclusion that the relative scattering efficiency of lysosomes and mitochondria does not very between cell types can be drawn from either graph. When the polarization is parallel to the scattering plane, lysosomes scatter roughly 20% more efficiently than mitochondria. When the polarization is perpendicular to the scattering plane, the increase jumps to roughly 60%.

#156183 - $15.00 USD Received 7 Oct 2011; revised 2 Dec 2011; accepted 30 Dec 2011; published 13 Jan 2012

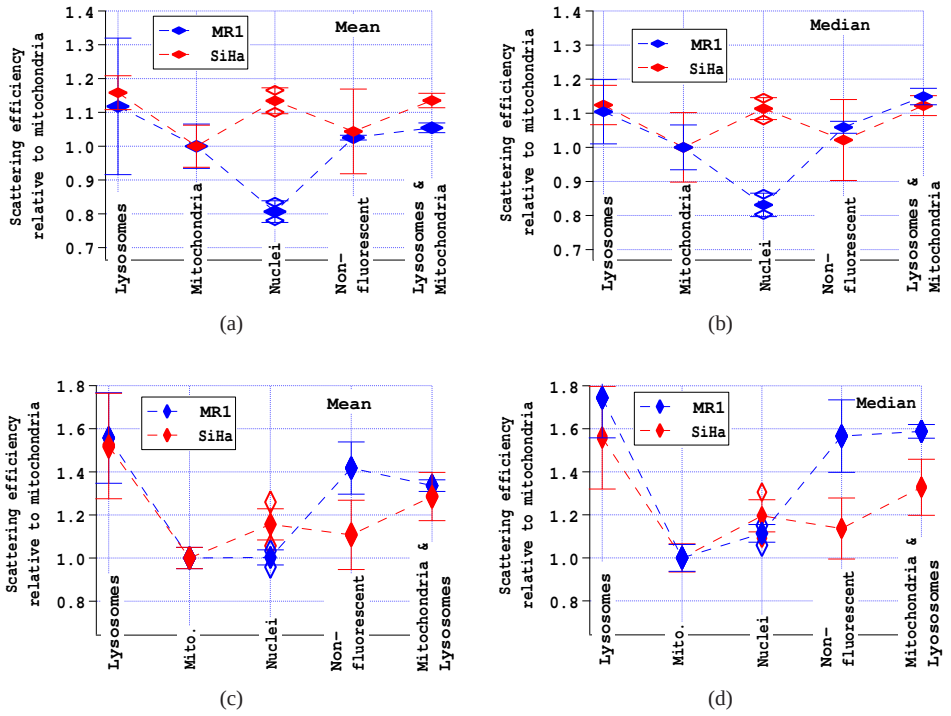

Fig. 8. Average and standard deviation of the mean and median of the distributions of scattering efficiencies normalized to the scattering efficiency of mitochondria. The plotted data are the averages of three or more experiments each with at least 3000 cells. a) and b) Average and standard deviation of the mean and median, respectively, for MR1 and SiHa cells with parallel polarization. c) and d) Average and standard deviation of the mean and median, respectively, for MR1 and SiHa cells with perpendicular polarization. The open symbols show the maximum and minimum nuclear scattering efficiency due to the uncertainty in the calculated increase in nuclear scattering due to Hoechst staining.

3.5. Percent of scattering from different organelles and structures

The percent of scattering from nucleus, mitochondria, lysosomes and the set of structures that were not stained was estimated as described in Section 2.4. The sum of the resulting calculations of scattering was 91 - 93%. Those calculations likely overestimated the contribution of the nucleus, because all area under the Hoechst mask was assigned to the nucleus regardless of overlap with other fluorescence. Consequently, equal amounts (2-3%) were added to the three other categories to make the sum 100%. The nucleus is clearly the largest contributor to side scattering in SiHa cells. The larger contribution of the nucleus to the SiHa cells than for the MR1 cells, is consistent with the nucleus being ∼26% of the volume of SiHa cells, while it is about ∼20% of the volume of MR1 cells. For MR1 cells, the contributions to scattering are more evenly distributed, with the nucleus and lysosomes likely being the strongest scatterers. In all cases, the contribution of the lysosomes is greater than the contribution of the mitochondria, with the difference being greatest for incident light with a polarization perpendicular to the scattering plane.

#156183 - $15.00 USD Received 7 Oct 2011; revised 2 Dec 2011; accepted 30 Dec 2011; published 13 Jan 2012

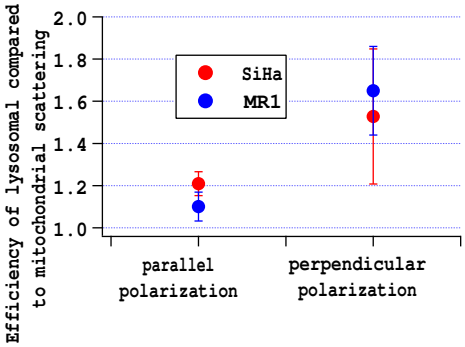

Fig. 9. Average and standard deviation (from 3 separate experiments) of the median of the distribution of scattering efficiency of lysosomes relative to that of mitochondria. The scattering efficiency of lysosomes was divided by the scattering efficiency of mitochondria on a cell by cell basis.

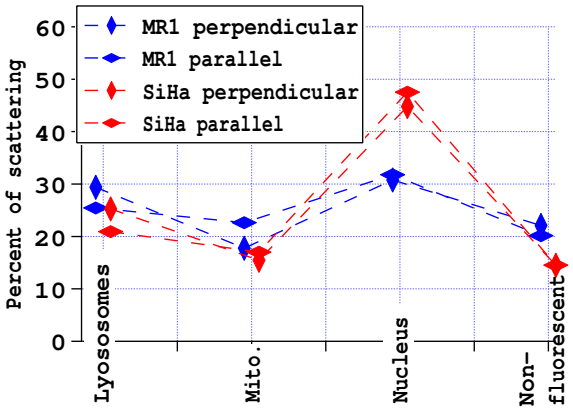

Fig. 10. Estimates of the percent of side scattering originating from each type of structure. The results are offset slightly for MR1 and SiHa cells for clarity.

4. Discussion

A goal of this work was to elucidate the relative scattering efficiencies of specific cellular organelles. The results clearly show that objects stained with LysoSensor Green are as efficient or more efficient than other cellular structures. We have assumed that LysoSensor Green only stains lysosomes, however, it should be noted that Lyosensor Green may not be specific to only lysosomes. LysoSensor Green DND-189 has a pKa of ∼5.2 and does not fluoresce at neutral pH. The fluorescence intensity increases with acidification. Several cellular organelles are acidic including the Golgi apparatus and lysosomes. The trans-Golgi network has a pH of ∼6.0 and recycling endosomes have a pH of less than 6.0. Secretory vesicles have a pH of ∼5.5 and lysosomes have a pH of ∼5.5 [23]. Therefore, while lysosomes are expected to exhibit the strongest fluorescence, secretory vesicles and recycling endosomes may have contributed to the fluorescence of LysoSensor Green.

For each experiment, there was a wide distribution of scattering efficiencies (see for example Fig. 6) as discussed in Section 3.4. The wide width of the distributions likely has at least two fundamental causes, scattering from different cellular structures and speckle. The 785 nm laser

#156183 - $15.00 USD Received 7 Oct 2011; revised 2 Dec 2011; accepted 30 Dec 2011; published 13 Jan 2012

used in this work is coherent and consequently generates speckle. This speckle may be the cause of some of the structure seen in the side scatter image and makes the interpretation of individual images difficult. However, by imaging and averaging results of thousands of cells in each experiment the intensity variations due to speckle should average out. A further advantage of averaging thousands of cells is that any effects on cell scattering due to cell orientation [24] are averaged out.

Throughout the paper, the assumption was made that scattering from regions with only a specific fluorescence was due only to that particular organelle. For example, scattering from regions with only MitoTracker fluorescence was assumed to be only due to mitochondria. In addition, however, there could have been a contribution to the scattering from nonfluorescent objects. This contribution can be estimated from Fig. 8c and d, in which scattering from the nonfluorescent particles was different for MR1 and SiHa cells. We assume that lysosomes and mitochondria have the same scattering efficiency in both cell types and that the contributions of nonfluorescent particles are the same in MitoTracker and LysoSensor fluorescing regions of both cell lines. The result is that nonfluorescent particles are $\sim$6 - 20% of the scattering efficiency from lysosomal and mitochondrial regions when the incident light is perpendicular to the scattering plane. Since, the nonfluorescent particles are more scattering than mitochondria, but less scattering than lysosomes, the difference between lysosomal and mitochondrial scattering efficiencies is probably greater than shown in Fig. 8.

Presented data support previous results that the nucleus is an efficient side scatterer. The nucleus is not homogeneous, but has many inhomogeneities [17] with a maximum chromatin clump size of about 1 μm [25]. FDTD simulations demonstrate that the greater the index of refraction variations within the nucleus, the more they scatter light at a wide variety of angles including 90° [25]. Additionally, in our own work modeling the angular distribution of scattering from nuclei, we found that homogeneous nuclei could not be used to explain the scattering from isolated nuclei - the scattering at 90° was significantly low (fig. 12 of [17]) and smaller scattering centers were needed to model the measured light scattering.

Wilson and Foster previously reported that lysosomes scatter approximately 14-15% of the light from EMT6 cells at 633 nm [26] while we estimate that lysosomes are 20–30% of the side scattering at 785 nm. Their results were based on measurements of angularly light scattering from $\sim$7° to 83° before and after the ablation of lysosomes. The contribution of lysosomal scattering to side scatter was found to be much greater in our work, between 20% and 30% depending on polarization and cell type. Our results may slightly overestimate the contribution of lysosomes due to the contribution of nonfluorescent particles (as discussed above). In comparing our work with Wilson and Foster, the facts that the wavelengths are different and that our work only looks at side scatter must be considered. Our data was taken at 785 nm versus Wilson and Foster's data at 633 nm. Generally, the contribution of smaller particles to scattering decreases as wavelength is increased and our data demonstrate that the scattering centers in lysosomes are small. Based on this comparison, our results would be expected to give a lower contribution of lysosomes. On the other hand, from Fig. 2 of Wilson and Foster [26], it can be inferred that lysosomes contribute more of the scattering at 90° than at angles less than 30°. Our results would, therefore be expected to show a higher contribution of lysosomes to scatter than was found by Wilson and Foster. Furthermore, our stain may have stained some low pH vesicles in addition to lysosomes. In conclusion, our results indicate a higher contribution of lysosomes to side scatter than the contribution to total scatter reported by Wilson and Foster.

A more profound difference between our results and previously reported results is the *relative* contribution of mitochondria and lysosomes to scattering. We found that not only are lysosomes much more efficient scatterers than mitochondria, lysosomes contribute at least as much and possibly more to side scatter in both MR1 and SiHa cells especially when the polarization is

#156183 - $15.00 USD Received 7 Oct 2011; revised 2 Dec 2011; accepted 30 Dec 2011; published 13 Jan 2012

perpendicular to the scattering plane. Wilson et al., however, reported about a 5 times greater contribution from mitochondria than from lysosomes to the total scattering cross section [13, 26]. Potentially, this discrepancy is due to the fact that Wilson et al. assumed that their light scattering signal was due to objects in the cytoplasm. Some of the scattering from particles that were assigned to mitochondria by Wilson et al. might be from the nucleus. We found that $\sim$30% of the side scattering from MR1 cells and $\sim$45% of the side scattering from SiHa cells was due to the nucleus.

The discrepancy between the result of Wilson et al. that mitochondria have a factor of 5 greater contribution to total scatter than total scatter than lyosomes and our result that lysosomes contribute similarly or slightly more to "side scatter" is unlikely to be primarily due to the fact that we measured side scatter while Wilson et al. [26] were measuring total scatter. Our measurements used a microscope objective with an NA of 0.75. Therefore we were collecting light over an angle range of $\sim 97^\circ$ centered at 90°. Consequently, for the ratios of total scatter, and side scatter to vary greatly, there must be a huge difference in the light scattering from mitochondria and lysosomes in the near forward or near backscattering directions. These differences are unlikely since mitochondria and lysosomes are similarly sized particles. Mitochondria are elongated particles which can vary in size with the cell cycle. Based on the results of Kennady et al. [27], the mitochondria in our MR1cells were roughly 0.7 to 3 μm long. Lysosomes are generally spheric or ovoid and vary in size from $\sim$1 μm to a little over a micron in many cell types including CHO (Chinese hamster ovary) cells [28]. In conclusion, the difference in some of the measurement angles between our work and that of Foster and coworkers may be the cause of some of the differences in results for the relative contribution of mitochondria and lysosomes. However, the inclusion of the nuclear contribution to side scattering in our work and possibly the inclusion of more low pH organelles (not just lysosomes) in the lysosomal contribution in our work likely contributed more to the differences in results.

In addition to providing insight into the fundamental question of what is scattering light, this paper also demonstrates some of the intrinsic advantages of measuring unstained/unprocessed samples over measuring stained samples. Images of stained samples can be used for localization of organelles and can provide beautiful pictures for insight into cellular phenomena. However, applications requiring the assumption that the dyes do not alter the cell should be undertaken with caution. In our case we found that Hoechst staining increases side scattering from the cells. Additionally, the size of SiHa cells increased when they were stained with all three of the dyes used. While it is beyond the scope of this paper to understand the biochemical interactions causing the changes in scattering or in cell size, the results demonstrate that frequently used stains have marked affects on the cells and that care must be used when interpreting results of experiments using fluorescent dyes.

5. Conclusions

1. Lysosomes are more efficient side scatterers than mitochondria, especially when the incident light is polarized perpendicular to the scattering plane.
2. Side scattering efficiency of unstained regions of the cells (i.e. regions not stained with Hoechst, MitoTracker or LysoSensor) is the same or greater than that of regions stained with MitoTracker. Unstained regions have a similar contribution to the total side scatter from MR1 and SiHa cells as mitochondria and lysosomes.
3. The nucleus contributes more than 40% of the side scattering from SiHa cervical carcinoma cells, but has a contribution of only $\sim$30% for MR1 fibroblast cells.
4. The relative side scattering efficiency of lysosomes and mitochondria does not appear to depend on cell type.

#156183 - $15.00 USD Received 7 Oct 2011; revised 2 Dec 2011; accepted 30 Dec 2011; published 13 Jan 2012

5. Some of the scattering centers in many organelles are much smaller than the organelle itself. The scattering centers in lysosomes and other low pH organelles are much smaller than the wavelength of light used (785 nm) as evidenced by the fact that they are much stronger side scatterers when the incident light polarization is perpendicular to the scattering plane.

Light scattering in mammalian cells is due to a wide variety of structure sizes [17, 29, 30]. Near forward scattering is related to size, while scattering at slightly larger angles is related to nuclear size [24] (and references within). As the scattering angle gets larger (out to $\sim 170^{\circ}$), the structures responsible for scattering generally get smaller [17]. These smaller structures sometimes reside in larger organelles such as the nucleus [25] and even the lysosomes. The nucleus, lysosomes, as well as particles unstained by Hoechst, LysoSensor or MitoTracker are each as significant for light scattering as mitochondria.

There are many applications of light scattering from biological cells, from cancer diagnosis in tissue to single cell measurements in flow cytometry to identify specific cell populations. This work provides fundamental information about light scattering for interpretation of data for these applications and may facilitate the development of new methods. Previously, it has been shown that the contribution of different structures to light scattering can be controlled by the choice of measurement angle [17, 24]. In this work, we have demonstrated that even at a single angle, 90°, the contribution of different organelles to light scattering can be controlled by the choice of polarization.

Acknowledgments

We thank Hongzhao Tian for performing the cell culture. This work was supported by National Institutes of Health grant CA071898 and by the Los Alamos National Flow Cytometry Resource funded by the National Center for Research Resources of NIH (Grant P41-RR01315).

#156183 - $15.00 USD Received 7 Oct 2011; revised 2 Dec 2011; accepted 30 Dec 2011; published 13 Jan 2012